Electrochimica Acta 446 (2023) 142121

Contents lists available at ScienceDirect

Electrochimica Acta

journal homepage: www.journals.elsevier.com/electrochimica-acta

Exploring the effect of surface chemistry and particle size of boron-doped diamond powder as catalyst and catalyst support for the oxygen reduction reaction

Gabriel Alemany-Molina [a], Beatriz Martínez-Sánchez [b], Atsushi Gabe [c], Takeshi Kondo [d], Diego Cazorla-Amorós [a], Emilia Morallón [b,*]

[a] Departamento de Química Inorgánica and Instituto Universitario de Materiales de Alicante (IUMA), University of Alicante, Ap. 99, Alicante 03080, Spain
[b] Departamento de Química Física and Instituto Universitario de Materiales de Alicante (IUMA), University of Alicante, Ap. 99, Alicante 03080, Spain
[c] Department of Biochemistry and Applied Chemistry, National Institute of Technology, Kurume College, Kurume, Japan
[d] Department of Pure and Applied Chemistry, Faculty of Science and Technology, Tokyo University of Science, Chiba, Japan

ARTICLE INFO

Keywords:
ORR
Boron-doped diamond powder
Iron-based catalysts

ABSTRACT

The interest for the electrodes based on conductive boron-doped diamond powder (BDDP) is increasing in recent years due to their excellent physical and chemical stability, the wide potential window in both aqueous and organic electrolytes, the relatively large specific surface area, and their versatility in comparison to boron-doped diamond thin film electrodes. These materials have been proposed as alternative cathode catalyst support due to their high corrosion resistance when subjected to the highly positive potentials originated during the start-stop operations in fuel cells, especially in automobiles. In this work, we present three BDDP supports with different particle sizes and different surface oxygen contents as supports of different iron species for oxygen reduction reaction in alkaline solution. BDDP supports were modified with carbon nitride (C_3N_4) or phthalocyanines (Pc) as anchoring points for iron. The different electrocatalytic performance observed confirmed the strong influence of the surface chemistry of the BDDP supports on the activity of the metallic sites for FePc samples while, for Fe-C_3N_4 samples, the determining effect was the particle size of the BDDP support. Additionally, DFT calculations were used to obtain some insights about the interaction of the FePc with the diamond surface.

1. Introduction

Fuel cells (FCs) convert chemical energy of fuel and oxidant into electric energy. Unlike batteries, they do not need recharging as long as fuel and oxidant are continuously supplied [1]. At the cathode of the FCs, oxygen is reduced to produce water ($1/2O_2 + 2H^+ + 2e^- \rightarrow H_2O$) [1] using an electrocatalyst. The sluggish reaction kinetics of Oxygen Reduction Reaction (ORR) even on the best Platinum-supported carbon (Pt/C) electrocatalyst requires high Pt loading (~0.4 mg cm^{-2}) to achieve a desirable fuel cell performance. While Pt/C is commonly used as a cathode catalyst for FCs, Pt is a scarce and expensive metal and the electrocatalyst suffers from the corrosion of carbon support and CO deactivation limiting the durability of FCs [2,3]. Especially, when applied to automobiles, the cathode catalyst is exposed to highly positive potentials during frequent start-stop operations, causing harsh deterioration by means of metal catalyst degradation and corrosion of carbon supports [2,3]. This deterioration results in a loss of Electrochemical Surface Area (ECSA), and consecutively a rapid failure of the device [4]. In this regard, cathode development requires special attention to find the best catalyst and electrode structure to combine performance and stability [5].

Boron-doped diamond (BDD) electrodes are known to exhibit wide potential window in aqueous and non-aqueous electrolytes, low background currents, and extreme physical and chemical stability [2,3]. BDD electrodes are usually prepared via chemical vapor deposition on different flat plate materials as BDD thin film. Therefore, it is difficult to obtain electrodes based on BDD with different shapes and configurations. Then, Boron-doped diamond powder (BDDP) may help to solve this problem [3]. BDDP electrodes obtained by growth of a BDD layer on the surface of diamond powder (DP) are suitable for electrochemical applications since it exhibits the sufficient electrical conductivity, large surface area and can be produced at large scale. Recently, Kim reported

* Corresponding author.
E-mail address: Morallon@ua.es (E. Morallón).

https://doi.org/10.1016/j.electacta.2023.142121
Received 29 September 2022; Received in revised form 24 February 2023; Accepted 25 February 2023
Available online 27 February 2023

that Pt/BDDP can be useful as a durable cathode catalyst for Polymer Electrolyte Membrane Fuel Cell (PEMFC). They fabricated a unit cell using the Pt/BDDP cathode catalyst and found that the decrease in Pt loading during an accelerated long-term test (0.6 V at 90ºC) was less on the BDD support than on the Vulcan XC-72 or multi-walled carbon nanotube supports [6]. Likewise, no changes in the voltammogram shape were observed for BDDP based ORR catalysts during a potentiostatic cyclic test [3]. BDDP is a potential candidate for durable catalytic support due to its nature of chemical inertness and thus can be applied to durable cathodic materials of FCs. Moreover, BDDP of the desired particle size can be easily obtained because the size of the DP substrate can be widely selected from the least several tens of nanometers to several tens of micrometers which can be an advantage when the supports are prepared with any metal contents. If transition metals are supported more strongly on the BDDP surface, a more durable cathode catalysts are expected to be obtained for FCs with improved stability with respect to the carbon support. Finally, the electrochemical characteristics of BDD based electrodes are known to depend on the type of surface termination (oxygen or hydrogen) [7–9]. It is inferred that total area of BDDP/electrolyte solution interface enabling a faster apparent electron-transfer rate for dopants at the BDDP electrode is dependent on surface chemistry of BDDP [7].

In this work, we present three BDDP with different particle sizes and different surface oxygen and hydrogen contents as supports of iron species in different arrangements of Fe-N_x type complex for ORR in alkaline electrolyte. Finally, the role of the chemical environment of the active sites and the interaction with the BDDP supports toward the ORR performance is investigated.

2. Experimental

2.1. Materials

Potassium hydroxide in pellets (KOH, 85% WWR Chemicals); Iron (III) nitrate 9-hydrate ($Fe(NO_3)_3{\cdot}9H_2O$, 99.99%, Sigma Aldrich); Dicyandiamide ($C_2H_4N_4$, Wako Pure Chemical Industries); 2-Propanol (C_3H_8O, 99.9%, Supelco); Nafion D-520 dispersion 5% w/w in water; 1-Propanol (Alfa Aesar). Iron(II) phthalocyanine (FePc, 90%) as well as platinum supported on a graphitized carbon material (20 wt% Pt) (named Pt/C) were used as received from Sigma-Aldrich. Fumion® FAA-3 was used as an anion exchange material (counter ion bromide) and was supplied by Fumatech BWT GmbH (Bietigheim-Bissingen, Germany). Isopropanol (C_3H_8O, 99.5%), was also purchased from VWR Chemicals. N, N-dimethylformamide (DMF), extra pure, was provided by Scharlau. All aqueous solutions were prepared with ultrapure water (18.2 MΩ cm, Millipore® Milli-Q® water). Nitrogen gas (N_2, 99.999%), oxygen gas (O_2, 99.995%) and (H_2, 99.999%) were supplied by Carburos Metálicos.

2.2. Preparation of BDDP materials

BDDP have been prepared using the procedure described elsewhere [3]. This procedure consists in depositing a BDD layer on the surface of a commercially available DP substrate by the microwave assisted plasma chemical vapor deposition method (MPCVD) [10]. The carbon impurities, consequence of the by-products of the CVD process, are removed by heat treatment in air at 425ºC for 5 h after the CVD process, which oxidizes the BDDP surface (O-BDDP). The BDDP surface is converted for hydrogen termination by hydrogen plasma treatment (H-BDDP) [7]. The nomenclature for O-BDDP and H-BDDP samples includes the particle size for each BDDP (i.e., O-BDDP-150 means O-BDDP with particle size of 150 nm).

2.3. FePc/BDDP and Fe-C_3N_4/BDDP preparation

O-BDDP and H-BDDP supports were modified with carbon nitride (C_3N_4) or phthalocyanines (Pc) as anchor points for transition metals. Specifically, iron (Fe) metal has been studied in this case. For the preparation of the carbon nitride modified materials, Fe precursor ($Fe(NO_3)_3{\cdot}9H_2O$) was introduced to obtain a nominal metal loading of 1 wt.% during the synthesis, using 15 wt.% of dicyandiamide as the C_3N_4 precursor. The samples were subjected to a 4 h heat treatment at 520ºC with a heating rate of 5ºC min^{-1} in N_2-atmosphere (150 mL min^{-1}), resulting in Fe-C_3N_4/H-BDDP-150, Fe-C_3N_4/O-BDDP-150 and Fe-C_3N_4/O-BDDP-650. On the other hand, commercial Fe phthalocyanines (FePc) were supported onto the BDDP substrates by using a widely used wet impregnation method. An appropriate amount of iron complexes dissolved in DMF (0.1 mg mL^{-1}) was mixed with the BDDPs to obtain a nominal metal loading of 1 wt.%. Afterwards, the solvent was evaporated by infrared light at 250 W for about 3 h, resulting in FePc/H-BDDP-150, FePc/O-BDDP-150 and FePc/O-BDDP-650 samples.

2.4. Physico-chemical, morphological and electrochemical characterization

The surface chemistry of the different samples was studied by temperature programmed desorption (TPD) experiments using a DSC-TGA instrument (TA Instruments, SDT 600 Simultaneous) coupled to a mass spectrometer (PRISMA PRO QMG 250 M1). The samples, previously dried at 120ºC for 1 h, were heated from 120ºC to 950ºC with a heating rate of 20ºC min^{-1}. The carrier gas used was He (100 mL min^{-1}). TEM micrographs were recorded with a transmission electron microscope model JEOL JEM-2010 (120 kV). X-ray Photoelectron Spectroscopy (XPS) was used to analyze the surface composition using a K-α spectrometer from Thermo Scientific, equipped with an Al anode.

Electrochemical characterization of the samples was performed in a three-electrode cell in 0.1 M KOH electrolyte at 25ºC and using an Autolab PGSTAT302 with a dual mode biopotentiostat module (Metrohm, Netherlands). Glassy carbon electrode surface (GC, 5.61 mm diameter, 0.25 cm^2) was employed as the working electrode (WE) for the electrochemical characterization in a rotating ring-disk electrode (RRDE, Pine Research Instruments, USA). Previously, GC was carefully polished with alumina slurries and rinsed with ultrapure water. Moreover, the RRDE is also equipped with a second annular working electrode, consisting of a Pt ring (0.19 cm^2). Moreover, a graphite bar (supplied by Mersen Ibérica) and a reversible hydrogen electrode (RHE) immersed in the same electrolyte in a Luggin capillary were used as a counter and reference electrode, respectively. The WE was prepared by dropping a 1 mg mL^{-1} dispersion of the catalysts ink in an aqueous solution (20 vol.% isopropanol and 0.02 vol.% Fumion® in water). The dispersion was previously homogenized via ultrasonication for at least 30 min. The amount of catalyst loading on the disk electrode was optimized in 0.48 mg cm^{-2}.

Electrochemical behavior in 0.1 M KOH N_2-saturated solution was first studied by cyclic voltammetry in a potential range from 0.0 V to 1.0 V at 50 mV s^{-1}. Then, the electrocatalytic performance of the materials towards the ORR was studied in 0.1 M KOH O_2-saturated electrolyte by linear sweep voltammetry (LSV), which consists of cycling between 1.0 V and 0.0 V at a scan rate of 5 mV s^{-1}. In addition, 20 wt.% Pt/C was also analyzed for comparison purposes. The potential of the Pt ring electrode was kept constant at 1.5 V during all measurements to ensure that the hydroperoxide anion (HO_2^-) reaching the Pt ring was oxidized. Then, the electrons transfer number (n) was determined as follows: $n = (4\ I_{disk})/(I_{disk} + I_{ring}/N)$, where I_{disk} and I_{ring} are the currents measured at the disk and ring electrodes, respectively, and N is the collection efficiency of the ring electrode that has been experimentally determined to be 0.37. The Tafel slopes were acquired from LSV experiments by plotting the potential vs logarithm of the current ($\log j_k$) at low overpotentials (reaction under kinetic control). Finally, long-term durability tests were carried out by cycling between 1.0 V and 0 V for 200 cycles and a rotation rate of 1600 rpm at 50 mV s^{-1}.

2.5. Density functional theory (DFT) calculations

Density Functional Theory (DFT) calculations at B3LYP/6–31 g level using Gaussian 16 software were carried out to understand and support the observed experimental results. The model structure consisted of a cluster of 82 carbon atoms with sp^3 hybridization saturated with hydrogen. The concentration of boron is low enough to be neglected. After, one of the terminal H was swapped to a terminal oxygen functional group and the interaction energy with a FePc macromolecule was studied. The model structure used for FePc consists of a macrocycle with four pyrrole units with four carbon atoms attached in the ring linked together by N bridges, and an iron metal atom coordinated with the pyrrole nitrogen atoms in the center of the ring. The changes in energies were calculated as the energy differences between the optimized structures of the final adduct and individual fragments energy and the energies are reported in eV (1 Hartree = 27.2114 eV).

3. Results and discussion

3.1. Physico-chemical and electrochemical characterization of BDDP

The SEM images, particle size distribution and conductivities of corresponding BDDP samples were described elsewhere [3]. As reported previously, the nanocrystalline BDD was deposited on the surface of the DP substrate during the CVD process and the obtained BDDPs showed a monomodal particle size distribution. The conductivities of BDDPs were around 10^{-1} S cm^{-1} which reveals that the BDDP can be used as an electrode material. The conductivity of BDDP increases with increasing the average particle size of BDDPs while the type of surface termination seems to affect little the electrical conductivities [7]. Indeed, the conductivity of O-BDDP-650 is much higher than that of O-BDDP-150 [3]. In addition, BET surface area of O-BDDP-150 is 106 m^2 g^{-1} which is a relatively low value compared to conventional amorphous carbon materials, revealing low amount of carbon edge sites.

Fig. 1 and Table 1 show the results obtained from the TPD experiments, in which the type and amount of gas evolved (mainly as CO or CO_2) and the decomposition temperatures correlate with the nature and amount of surface oxygen functional groups. The total amount of O (Table 1) confirmed that the reduction treatment by MPCVD was effective as it was reduced by about a quarter from initial O-BDDP-150 to H-BDDP-150. Furthermore, O-BDDP-650 sample presented a lower amount of CO and CO_2-type groups than O-BDDP-150, which is coherent considering the lower surface area of this sample. According to the results from CO desorption (Fig. 1), O-BDDP samples present mainly phenol and ether-like groups (600–750ºC), as well as carbonyl groups (650–950ºC), whereas H-BDDP sample contains few oxygen functional group of high stability. The presence of pyrone-type groups cannot be discarded [11–13]. As can be observed from TPD deconvolution of CO desorption (Fig. S1), phenol-like species are the most abundant surface oxygen groups on O-BDDP other than those present in the reduced sample (H-BDDP). Furthermore, O-BDDP samples contain some lactone groups (550–800ºC) while they are not observed in H-BDDP sample from CO_2 desorption.

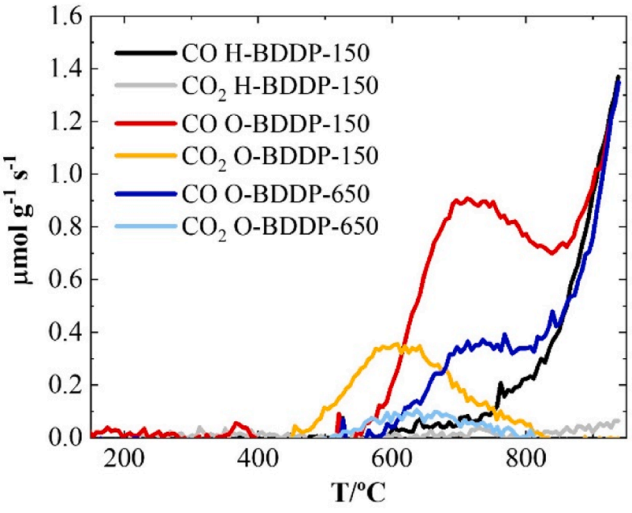

Fig. 1. TPD experiments for BDDP samples (20ºC min^{-1} and 100 mL min^{-1} He). *(an online color version should be used).*

Table 1
Surface chemistry characterization obtained from the TPD experiments.

Sample	CO (µmol/g)	CO_2 (µmol/g)	Total O (µmol/g)
H-BDDP-150	300	–	300
O-BDDP-150	800	220	1240
O-BDDP-650	430	45	520

Fig. 2a shows the cyclic voltammograms (CVs) of the BDDPs. The double layer observed for O-BDDP-150 is larger than for H-BDDP-150 due to the higher presence of surface oxygen functional groups, which increased the wettability. Furthermore, the double-layer current observed for O-BDDP-650 was lower than for O-BDDP-150 because of its lower surface area. Fig. 2b shows the LSV obtained for these BDDPs during ORR. All electrodes show a low electrochemical activity for this reaction; however, the O-BDDP-650 shows lower limiting current density, n and onset potential for ORR than H-BDDP-150 and O-BDDP-150. It is known that the activity of carbon edge sites is much higher than those of carbon basal planes toward ORR [14,15]. Thereby, the lowest ORR activity of O-BDDP-650 is because of the lower amount of carbon edge sites due to its larger particle size than H-BDDP-150 and O-BDDP-150. Zhong et al. reported that a combination of the carbon edge sites and electron transfer resistance ultimately determine the ORR performance [16]. In case of BDDPs prepared in this work, the edge carbons seem to dominate the ORR due to the low electron transfer resistance of BDDPs [16].

When the activities of H-BDDP-150 and O-BDDP-150 samples are compared, limiting current density of H-BDDP-150 is slightly higher than O-BDDP-150 while the onset potentials of these samples are similar. Since H-BDDP-150 is a sample reduced by hydrogen, it seems that ORR activity is slightly decreased by oxygen containing functional groups on BDDPs [17]. Overall, the particle size of BDDPs seem to be a more dominant factor than those of surface chemistry in BDDP samples for ORR activities.

3.2. BDDP as catalyst support for ORR

Due to the extraordinary properties mentioned above, such as wide stability potential window and low background current, BDDP substrates can be also applied as a model carbon support for fundamental electrochemical and electrocatalytic studies. This section presents the modification of H-BDDP-150, O-BDDP-150 and O-BDDP-650 samples with carbon nitride (C_3N_4) or phthalocyanines (Pc) as anchor points of active catalytic sites. Specifically, iron species are studied in two different arrangements of Fe-N_x type complexes (Fe-C_3N_4 and FePc) to deeply understand the role of the chemical environment of the active sites and the interaction with the BDDP supports in the electrocatalytic performance. It is worth noting the relevance of the chemical nature of the environment of the central metal atom, which must be carefully selected for the reaction under study.

Macrocyclic metal complexes are widely known as electron transfer mediators for multiple reactions [18]. During the last few years, iron metal on M-N_4 systems have shown remarkably prominent performance towards the ORR. Due to their excellent catalytic behavior and electrochemical richness, they have been extensively studied for different applications especially as electrocatalysts for fuel cell devices and have

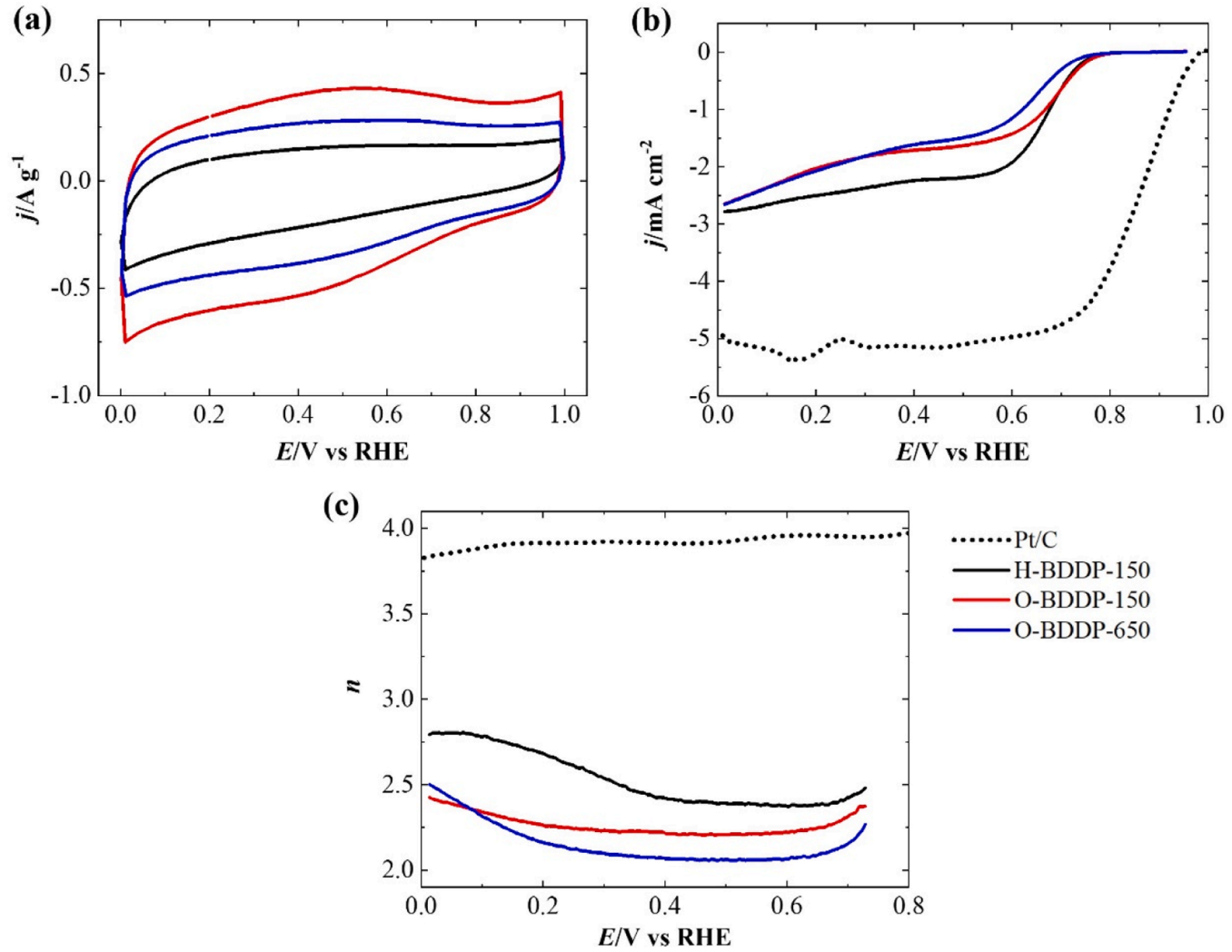

Fig. 2. (a) Cyclic voltammograms in N_2 atmosphere in 0.1 M KOH electrolyte, (b) LSVs during ORR on the disk electrode and (c) number of electrons transferred per oxygen molecule for the different BDDP and the commercial Pt/C catalyst recorded in O_2-saturated 0.1 M KOH solution at electrode rotation rate of 1600 rpm. Scan rate of 5 mV s^{-1}. *(an online color version should be used).*

been supported on a wide variety of carbon-based materials in recent years [19]. However, from the best of our knowledge, this is the first time that Fe-N_x based samples are studied from a fundamental point of view supported on BDDP substrates with different size and surface chemistry.

3.2.1. Structural and morphological characterization of Fe-C_3N_4/BDDP and FePc/BDDP composites

The structural and morphological properties of the Fe-C_3N_4/BDDP and FePc/BDDP composites were analyzed by Raman spectroscopy and TEM measurements. Firstly, Raman results in Fig. S2 show slight changes of all BDDP spectra when Fe-catalysts were supported. Fig. S2b, c reveal two main contributions at 1340 cm^{-1} and 1600 cm^{-1}, for both H- and O-terminated BDDP substrates with the same particle size (H-BDDP-150 and O-BDDP-150, respectively), before and after supporting the Fe-species, which are directly associated with the D and G-bands for graphite-related materials [20,21]. In addition, 2D and $D + G$ characteristic modes at around 2700 cm^{-1} and 2900 cm^{-1} [22] are also observed in the second order region in the Raman spectra in Fig. S2a for these samples. These results suggest that both BDDP-150 supports contain Csp^2 graphitic impurities, probably as by-products of the CVD treatment [3,23]. After the incorporation of FePc molecules, the width of the D band increases. The presence of a shoulder at around 1500–1550 cm^{-1} and small wide bands at around 1750 cm^{-1} and 2070 cm^{-1} can be also related to interstitial disorder/defect sites and structural changes due to the interaction between FePc molecules and surface C atoms. Nonetheless, π-π stacking interactions between the aromatic system of FePc molecules and the graphitic residues should not be ruled out. Interestingly, the increase of the width of the D band observed for Fe-C_3N_4/BDDP-150 samples was slightly higher than that observed for the FePc modified materials. This is in agreement with the higher size of a C_3N_4 flake in comparison with Pc, that might be forming polymeric domains over the BDDP particles. Furthermore, the characteristic 2D and $D + G$ modes were not observed in Fe-C_3N_4/BDDP samples.

Interestingly, O-BDDP-650 substrate, with the highest particle size, shows a very different pattern in Fig. S2d. A sharp band centered at around 1320 cm^{-1} can be observed related to diamond Csp^3 contribution [23], which means that the content of graphite domains was lower compared to BDDP-150 supports. In this case, FePc loading did not modified the spectrum significantly. However, when C_3N_4 is synthesized over the O-BDDP-650 support, the band observed is broad and it is centered at frequencies corresponding to Csp^2 contribution. This implies that the C_3N_4 sheets might be efficiently covering the BDDP surface, especially when it is synthesized over particles with larger sizes. Therefore, the particle size seems to significatively affect the structural quality of BDDP supports and, consequently, their interaction with the

iron species.

Fig. S3 shows TEM images of BDDP supports and BDDP modified composites. Comparing H-BDDP and O-BDDP substrates (Figs. S3a-c), the surface of O-BDDP is rough due to their higher degree of oxidation while H-BDDP-150 showed a smoother morphology. Some dark aggregates are observed in FePc/H-BDDP-150 with a particle size between 2 and 3 nm, while for FePc/O-BDDP-150 aggregates presented higher particle sizes (3–4 nm) due to partial aggregation of FePc molecules (Figs. S3d-f). This might indicate a worse distribution of the FePc molecules in the presence of the oxygen functional groups. For FePc/O-BDDP-650 catalyst, no clear agglomeration is observable by TEM. On the other hand, Fe-C_3N_4/BDDP samples (Figs. S3g-i) did not show significant differences compared to the pristine materials (Figs. S3a-c). Metal nanoparticles detectable by TEM were not observed, so iron species seem to be highly dispersed and stabilized by the C_3N_4-type domains formed.

The presence of C_3N_4-type species was confirmed with the N 1 s XPS spectra for the Fe-C_3N_4/BDDP samples (Fig. S4). N 1 s spectra for C_3N_4 can be deconvoluted into three peaks [24,25]. The contributions to the spectra presented equivalent binding energies to bare C_3N_4 (398.6, 399.8, and 401.0 eV). The presence of iron induced higher contributions than bare C_3N_4 for the peak at ~399.8 eV since N bonded to metal as M-N_x species show a contribution at around 399.5 eV [26].

3.2.2. *Electrochemical characterization*

3.2.2.1. Fe-C_3N_4/BDDP. CVs of the Fe-C_3N_4 modified samples are presented in Fig. 3a. The double layer charge observed for all the samples was higher after the modification with the C_3N_4 species, especially for BDDP-150 samples (Fig. 2a and Fig. 3). This might be related to the introduction of some rugosity in the surface of the BDDP particles because of the formation of C_3N_4-type nanodomains, and to a modification of the wettability due to the presence of nitrogen polar groups in the C_3N_4 that may increase the hydrophilicity.

The asymmetric like shape of the CV for C_3N_4/O-BDDP-150 sample (Fig. 3b) agrees with some pseudocapacitance contribution, like what is observed in N-containing carbon materials in alkaline conditions [27, 28]. CV of Fe-C_3N_4/O-BDDP-150 sample compared to C_3N_4/O-BDDP-150 (Fig. 3b), reveals that the faradic contribution observed at around 0.2 V can be related to the Fe^{II}/Fe^{I} redox process [29, 30]. Interestingly, Fe^{III}/Fe^{II} redox process was only observed for Fe-C_3N_4/O-BDDP-650 at around 0.7 V (Fig. 3a), which might indicate a different Fe chemical environment when C_3N_4 is prepared over larger particles (~650 nm). For BDDP-150 samples (Fig. 3b), Fe^{III}/Fe^{II} transition seems to be unfavorable while Fe^{II}/Fe^{I} transition was clearly observed. Interestingly, the cathodic peak potential of the Fe^{III}/Fe^{II} transition is an important factor for describing the catalytic activity of FeN_4 systems towards the ORR [31]. The fact that this redox process was only observed for Fe-C_3N_4/O-BDDP-650 suggests that this may be the electrocatalyst with the higher activity for this reaction. However, the low potential value for this material (Table 2) may indicate that, compared to FePc samples (see below), this is the electrocatalyst with the poorest charge transfer between the substrate and the redox species, which usually leads to poor catalytic performance.

Regarding the electrocatalytic activity towards the ORR, all samples improved E_{ONSET} potentials in at least 50 mV when BDDP supports were decorated with Fe-C_3N_4 species (Table 2 and Fig. 3c). Although relatively high E_{ONSET} potentials were achieved (up to 0.85 V), low current densities were obtained for BDDP-150 samples. The current density was limited by the selectivity with values close to 50% production of H_2O_2. The differences in selectivity between Fe-C_3N_4/H-BDDP-150 and Fe-C_3N_4/O-BDDP-150 were similar to those observed for the supports (H-

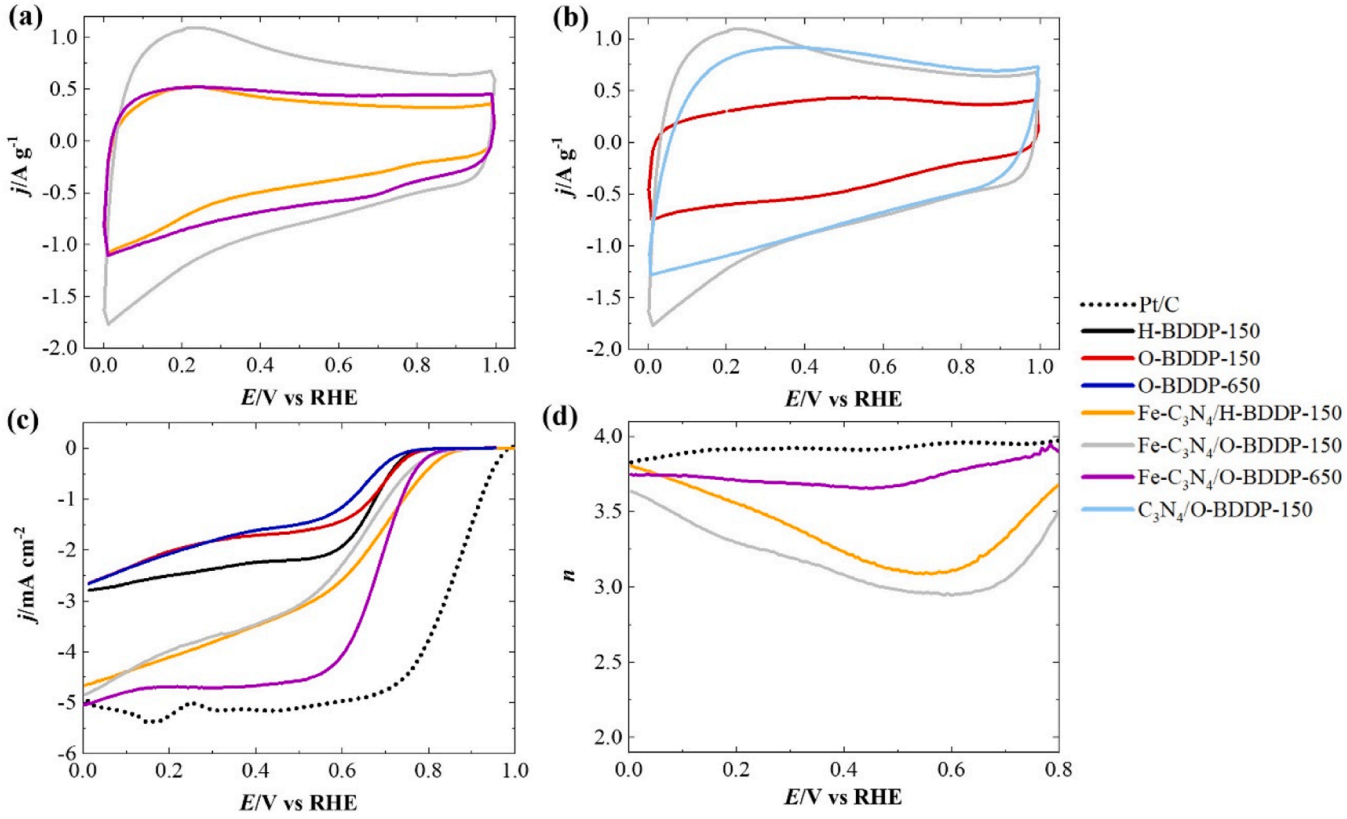

Fig. 3. (a) Cyclic voltammograms for Fe-C_3N_4 modified samples and (b) O-BDDP-150, C_3N_4/O-BDDP-150 and Fe-C_3N_4/O-BDDP-150, recorded in N_2-saturated 0.1 M KOH at 50 mV s^{-1}. (c) ORR polarization curves and (d) number of electrons transferred (n) per oxygen molecule derived from the RRDE tests during the ORR in O_2-saturated 0.1 M KOH solution at electrode rotation rate of 1600 rpm. Scan rate of 5 mV s^{-1}. *(an online color version should be used).*

Table 2
Electrochemical data of H-BDDP-150, O-BDDP-150, O-BDDP-650 and each respective composite with FePc molecules, together with comparison with Pt/C, in N_2 or O_2-saturated 0.1 M KOH solution.

Catalyst	E^0 (Fe^{III}/Fe^{II}) (V vs RHE)	E_{ONSET}[a] (V vs RHE)	n[b]	Tafel slope (mV dec^{-1})
Pt/C	–	0.97	3.9	55
H-BDDP-150	–	0.76	2.4	80
O-BDDP-150	–	0.77	2.3	80
O-BDDP-650	–	0.74	2.2	78
Fe/C_3N_4/H-BDDP-150	–	0.85	3.4	61
Fe/ C_3N_4/O-BDDP-150	–	0.82	3.1	75
Fe/ C_3N_4/O-BDDP-650	0.70	0.79	3.8	72
FePc/H-BDDP-150	0.82	0.92	3.9	35
FePc/O-BDDP-150	–	0.89	3.9	72
FePc/O-BDDP-650	0.79	0.86	3.8	61

[a] Determined at −0.1 mA cm^{-2},
[b] Determined at 0.7 V vs RHE.

BDDP-150 and O-BDDP-150, respectively) (Fig. 3d); then, the selectivity of Fe-C_3N_4/BDDP-150 samples may correspond to the combination of the contribution of BDDP sites and Fe-N_x sites, which usually behave as 4-electron pathway sites [32–35]. Therefore, part of the BDDP surface is probably not covered by the C_3N_4 domains. However, Fe-C_3N_4/O-BDDP-650 sample presented an excellent selectivity towards the 4-electron pathway, which is especially remarkable considering that O-BDDP-650 has the highest selectivity between the three BDDP supports towards the 2-electron pathway. This suggests that, in this case, Fe-C_3N_4 domains cover most of the BDDP surface as suggested by Raman characterization. The current density achieved by this sample is comparable to the commercial Pt/C electrocatalyst (Fig. 3c) but the E_{ONSET} potential is quite lower. These observations agree with other investigations which indicate that Fe-C_3N_4 might not be as active as other transition metals (e.g., Cu-C_3N_4 or Ni-C_3N_4) [36,37].

Tafel plots are shown in Fig. S5. BDDP samples before modification showed equivalent Tafel slopes. After the modification with the Fe-C_3N_4 species, the electron transfer was improved in all the samples as expected due to the high affinity of Fe-N_x sites for O_2. Nevertheless, the different surface chemistry of H-BDDP-150 and O-BDDP-150 samples induced changes in the electron transfer, where the reduced surface of Fe-C_3N_4/H-BDDP-150 led not only to the best E_{ONSET} but also to an improved electron transfer compared to Fe-C_3N_4/O-BDDP-150. However, despite the improvement of the E_{ONSET}, Fe-C_3N_4/H-BDDP-150 sample activity was very limited due to the non-homogeneous covering of the BDDP nanoparticles. The lowest Tafel slope value was observed for Fe-C_3N_4/O-BDDP-650; this suggests that for this electrocatalyst the homogeneous formation of Fe-C_3N_4 in the larger BDDP particles is a more relevant parameter than the surface chemistry of the BDDP materials. The fact that the influence of the surface chemistry in the catalytic activity of the Fe-C_3N_4 samples is minimal compared to the effect of the particle size may be related to the heat treatment applied for the synthesis. At the synthesis temperature, the interactions with the oxygen functional group might be less relevant while the size of the BDDP nanoparticle is what truly determined the quality of the C_3N_4 sheet formed and, therefore, the catalytic activity of the iron species.

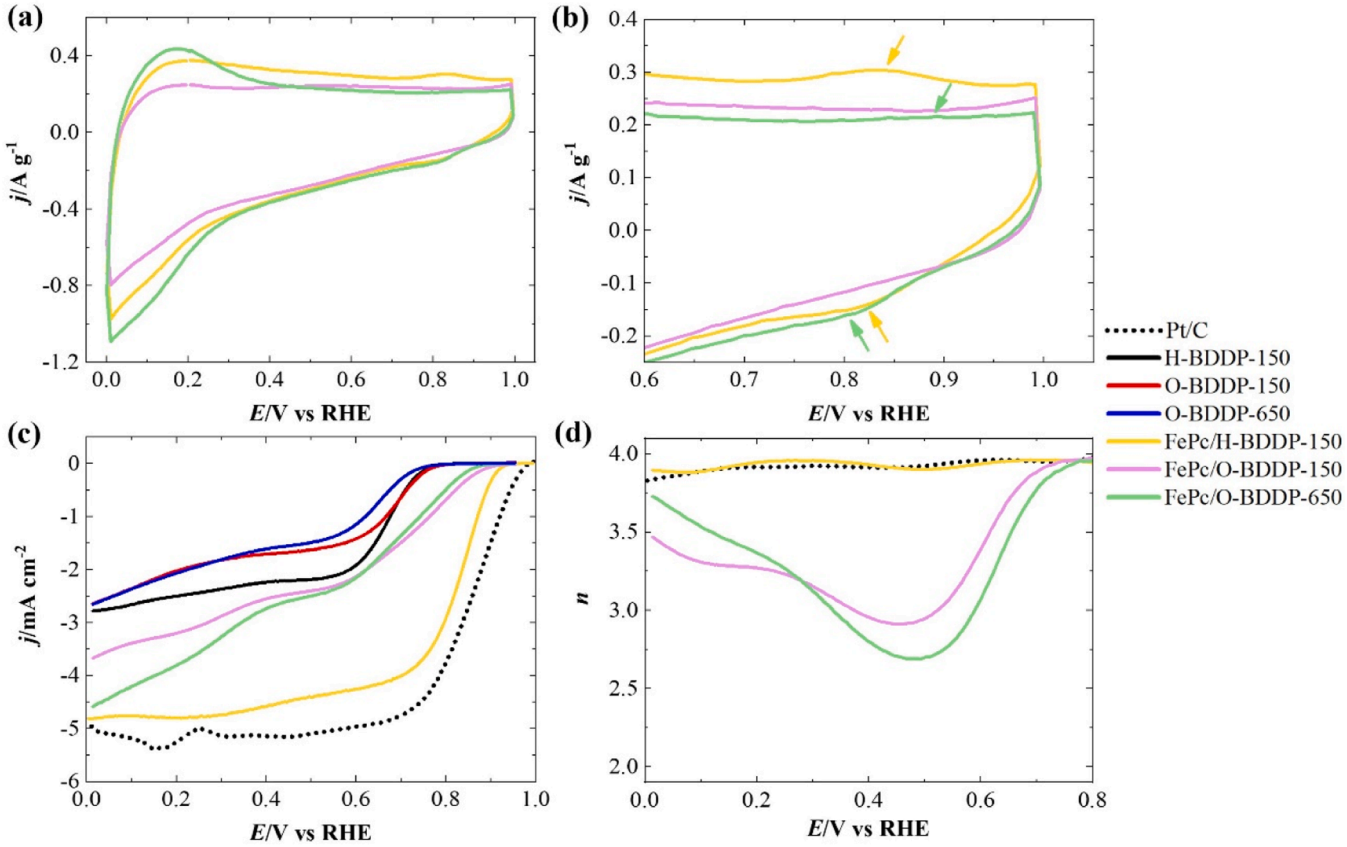

Fig. 4. (a) Cyclic voltammograms and (b) magnification of the CVs in (a) in the potential range of Fe^{II}/Fe^{III} redox process of FePc/H-BDDP-150, FePc/O-BDDP-150 and FePc/O-BDDP-650 samples, recorded in N_2-saturated 0.1 M KOH at 50 mV s^{-1}. (c) ORR polarization curves and (d) number of electrons transferred (n) per oxygen molecule derived from the RRDE tests during the ORR for Pt/C, H-BDDP-150, O-BDDP-150, O-BDDP-650, FePc/H-BDDP-150, FePc/O-BDDP-150 and FePc/O-BDDP-650 catalysts in O_2-saturated 0.1 M KOH solution at electrode rotation rate of 1600 rpm. Scan rate of 5 mV s^{-1}. *(an online color version should be used).*

3.2.2.2. FePc/BDDP. Fig. 4 shows the electrochemical behavior and the RRDE measurements towards the ORR for the FePc/H-BDDP-150, FePc/O-BDDP-150 and FePc/O-BDDP-650 electrocatalysts, in N_2 and O_2-saturated 0.1 M KOH electrolyte, respectively. The electrochemical and electrocatalytic responses of the commercial Pt/C catalyst is also shown in Figs. 4c,d for comparison purposes.

Firstly, the electrochemical CV profiles in Figs. 4a,b show a high sensitivity to the surface termination and the size of the BDDP substrates used as catalyst support. Typically, FePc molecules also originate two redox processes due to the metal center and related to Fe^{II}/Fe^{I} and Fe^{III}/Fe^{II} transitions [29,30], in which the cathodic peak potential of the last process (i.e., Fe^{III}/Fe^{II} transition) is an important factor for describing the electrocatalytic activity towards the ORR [31], as it has been mentioned above. It is worth mentioning that the first redox process (Fe^{II}/Fe^{I}) is shifted in all FePc-containing samples towards less positive potentials compared to previous studies in alkaline electrolyte [38,39], possibly induced by the effect from the BDDP substrate regardless of their surface chemistry. Interestingly, the second redox process (Fe^{III}/Fe^{II}) (oxidation and reduction peaks marked with colored arrows in Fig. 4b) seems to be less favored when O-BDDP substrates are used as support, since it has been previously demonstrated that oxygen functional groups in BDD seem to be detrimental to charge transfer between the substrate and the redox species [40]. Accordingly, this effect is especially evident for the FePc/O-BDDP-150 catalyst, in which Fe^{III}/Fe^{II} redox peaks are not clearly distinguished, in close agreement with the higher oxygen content of the O-BDDP-150 support determined by TPD measurements. Furthermore, the amount of Fe electrochemically active (Fe^{II}/Fe^{I} transition) is also lower for this sample, which might be related to higher aggregation of FePc in presence of a larger amount of surface oxygen functional groups. In this sense, Fe^{III}/Fe^{II} voltametric redox peaks are more reversible and well-defined on H-BDDP-150 support under the studied conditions, indicating faster electron transfer and both better interaction and distribution of FePc molecules.

Unlike the Fe-C_3N_4 catalyst, the effect of the surface chemistry of the BDDP support plays a critical role when FePc is used. As mentioned above, the reduced support H-BDDP-150 offers the best conditions for FePc catalyst, where it seems that the active iron sites are more available with no significant influence of the remanent oxygen functional group in the support. However, the lower catalyst-support interaction could also be adverse for the long-term stability of the catalyst. Despite several reports in the literature have studied the incorporation of oxygen functional groups on sp^2-carbon-based supports as anchor points for axial coordination of FePc molecules [38,41], the present work suggests a better response of FePc molecules on reduced BDDP substrates. In this sense, although some specific oxygen functional groups have been proposed to coordinate with FePc molecules (especially C-O-H or C-O-C species) [38,41], the catalytic results in Fig. 4 suggest that such axial coordination on BDDP support does not have a beneficial contribution, which could promote strong interactions in localized points on the surface oxygen functional groups, leading to higher stacking of FePc molecules and, therefore, lower amounts of electrochemically active iron . Nonetheless, it should be mentioned that the presence of some content of oxygen functionalities is also essential to improve the wettability and electroactivity in aqueous solvents [42–44]. Actually, some studies have also proven a fast electron transfer and more stable electrochemical responses for O-terminated BDD electrodes than for H-terminated ones despite the additional surface conductivity provided by H-termination [45]. However, different preparation factors should be optimized (i.e., boron content, low nondiamond carbon, etc.). Therefore, a compromise must be reached between the amount of incorporated oxygen functional groups and the proper electron transfer of the resulting BDDP support to achieve an optimal interaction with other redox species, such as FePc molecules, together with a good electrochemical response. This compromise seems to be superior for FePc molecules when supported on H-BDDP-150, which is the support with the lower amount of oxygen functional group.

In general, a clear improvement of the ORR performance is seen for all Fe-related samples in terms of E_{ONSET} and selectivity towards the most energy efficient 4-electron process for the ORR in alkaline medium, compared to the BDDP substrates. The electrochemical parameters derived from the RRDE measurements are also listed in Table 2 and compared to the commercial Pt/C electrocatalyst. Contrary to what was observed for Fe-C_3N_4 based materials, the observed catalytic differences for FePc samples suggest a greater influence of the surface chemistry of the BDDP support on the electrocatalytic performance.

Specifically, FePc supported on H-BDDP-150 shows the best catalytic activity with an onset potential of 0.92 V and an extraordinary selectivity towards the 4-electron pathway, with a catalytic behavior close to the commercial Pt/C catalyst. Contrary to what was observed for Fe-C_3N_4/H-BDDP-150 sample, the reaction is completely determined by Fe active sites as the selectivity observed in the whole range of potential noticeably corresponds to FePc complexes and the limiting current density is reached at around 0.75 V. These results showed that the H-BDDP-150 support is probably homogeneously covered with FePc molecules because the contribution of the BDDP sites was not observed. These promising electrocatalytic results are also supported by the lowest Tafel slope (at low overpotentials, i.e., kinetic control region) seen in Fig. S5 and reported in Table 2. Tafel slopes close to 40 mV dec^{-1} are expected for FePc systems in which the dioxygen molecules adsorption/activation is the rate-determining step [46]. Higher values of Tafel slopes are observed for FePc/O-BDDP-150 and FePc/O-BDDP-650, which indicate a poorer electron transfer during the ORR in the presence of oxygen functional groups [17]. Therefore, a low amount of oxygen functional group in the H-BDDP-150 support for decorating FePc seems to be an important factor for achieving higher catalytic activities. For FePc/O-BDDP samples, the contribution of the support to the selectivity is clearly observed (Fig. 4d), which might be related to a less homogeneous distribution of the FePc.

Regarding the effect of the particle size of the BDDP support, it is also important to mention that FePc/O-BDDP-150 catalyst did not display the Fe^{III}/Fe^{II} redox transition (Figs. 4a,b) and the amount of Fe electrochemically active seems to be lower than that of FePc/O-BDDP-650 sample. E_{ONSET} potentials were similar but FePc/O-BDDP-650 sample reached higher current densities at high overpotentials, which is in good agreement with the higher amount of Fe electrochemically active observed in CV experiments. This may be related to the larger size of the O-BDDP-650 particles, that may allow a better distribution of FePc complexes with less aggregation. Therefore, the performance of FePc is mainly determined by the surface chemistry, although the particle size of the BDDP support shows some influence on the catalytic behavior towards the ORR.

3.2.2.3. Stability tests. Once the effect of the surface chemistry and the particle size of BDDP supports have been discussed in depth in the previous sections, the materials with the best electrocatalytic performance, both from FePc and Fe-C_3N_4-related samples, were submitted to stability tests under operating conditions. In the light of the previous comments, despite the best electrocatalytic results are observed for FePc/H-BDDP-150, the poor interaction of FePc macromolecules with the H-terminated BDDP electrodes has triggered a clear drop in its catalytic performance after operating for 200 cycles (Fig. 5) in terms of E_{ONSET}, limiting current density and selectivity. Therefore, changes in the nature or lixiviation of the active sites are not ruled out after 200 cycles. Much better results are observed for Fe-C_3N_4/O-BDDP-650 catalyst with a catalytic behavior that remained almost unchanged after the stability test, which indicates that the chemical environment of the active sites should be of the same nature as before the test. As mentioned above, the catalyst-support interaction is key for long-term stability of the catalysts, so the heat treatment applied for the synthesis of the Fe-C_3N_4 may have induced a strong interaction with the support, preventing the dissolution of the iron species. TEM images after the stability

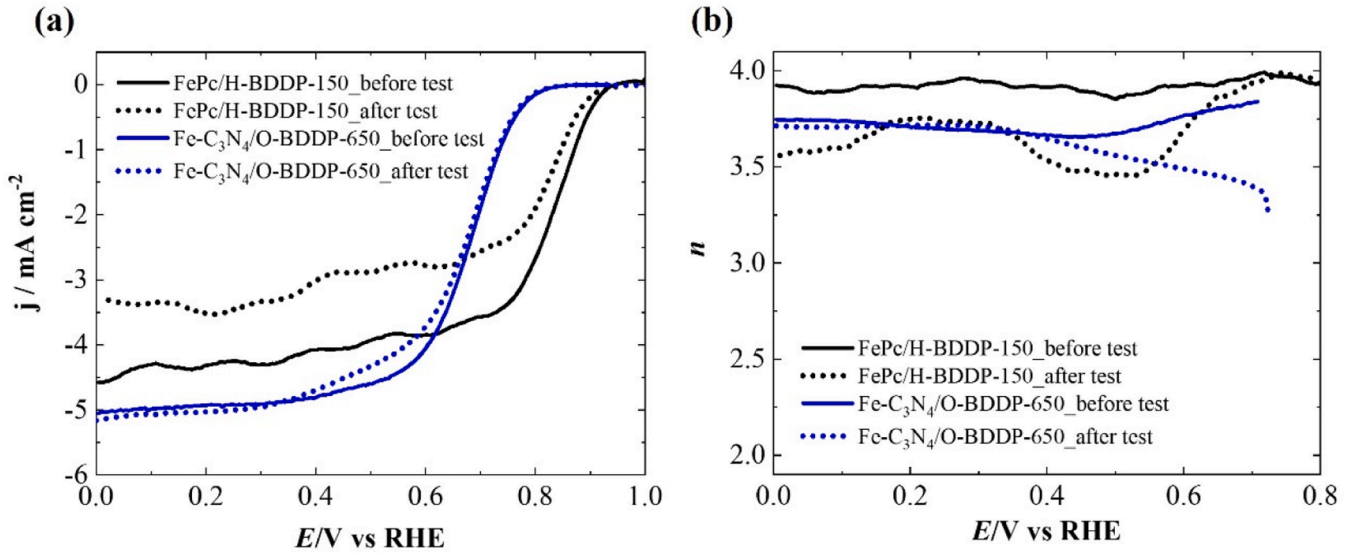

Fig. 5. (a) LSV durability test and (b) number of electrons transferred per oxygen molecule derived from the RRDE tests during the ORR for FePc/H-BDDP-150 and Fe-C_3N_4/O-BDDP-650 samples, before and after 200 cycles, in O_2-saturated 0.1 M KOH solution at electrode rotation rate of 1600 rpm and a scan rate of 50 mV s^{-1}. *(an online color version should be used).*

test are displayed in Fig. S6. The absence of small aggregates in Fig. S6a, compared to Fig S3d, confirms the lixiviation of iron for FePc/H-DBBP-150 catalyst after 200 cycles under operating conditions. Interestingly, TEM image for Fe-C_3N_4/O-BDDP-650 (Fig. S6b) does not show significant differences compared to the catalyst before the reaction (Fig. S3i) and to the support (Fig. S3c), what indicates that there are not significant changes in the electrocatalyst after the stability test, what is in agreement with the observed stability. In view of these results, it could generally be stated that H-termination provides higher surface conductivity, which is beneficial for ORR activity, but the interaction with the

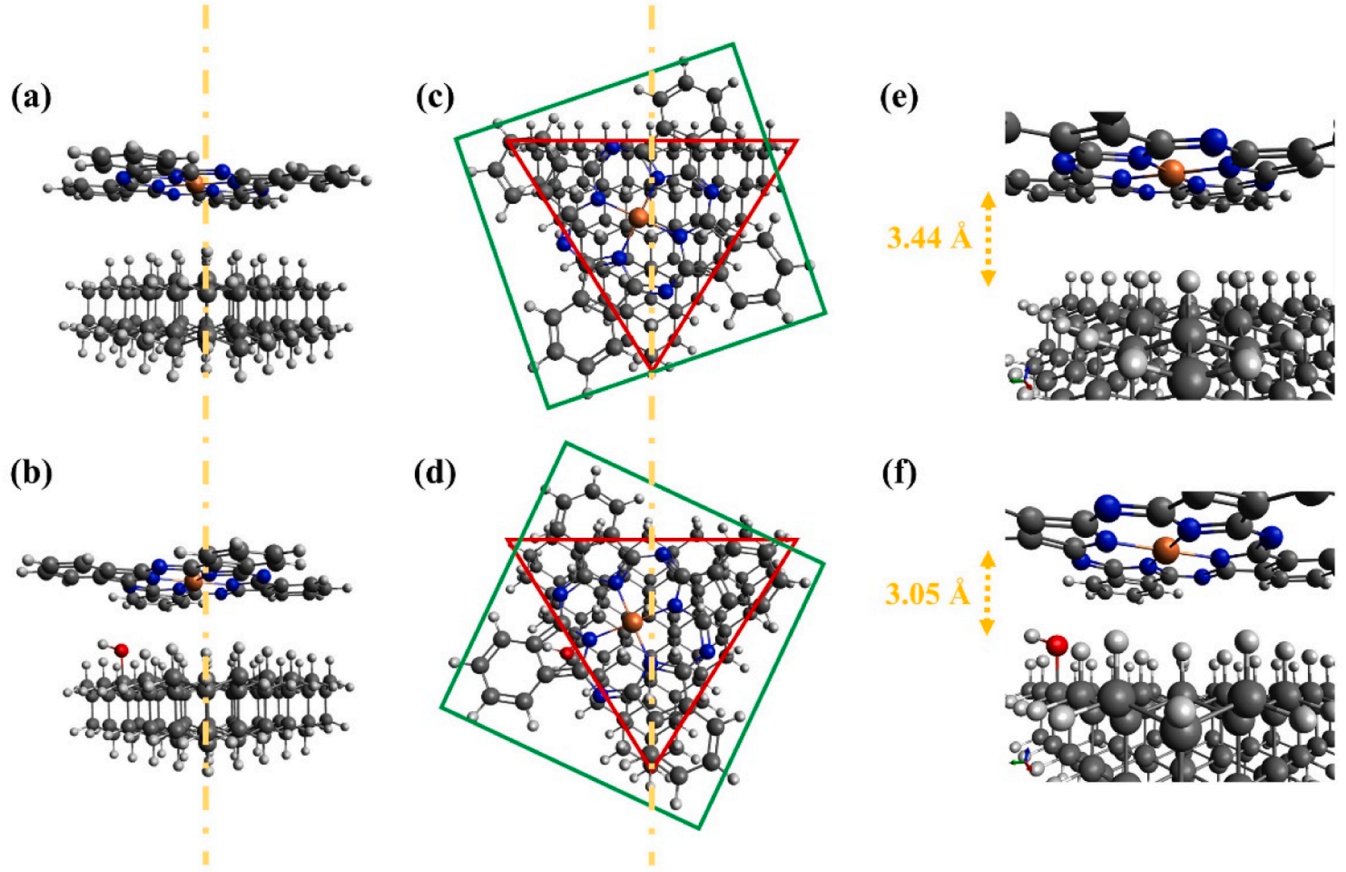

Fig. 6. Optimized molecular structures of FePc interacting with a H-saturated and -OH substituted diamond cluster. H is white, C is gray, N is blue, O is red, and Fe is orange. *(an online color version should be used).*

FePc is not strong enough to obtain a stable catalyst. Nevertheless, low-temperature treatments can be used to extend phthalocyanine-based catalysts to long-term applications [47].

Furthermore, chronoamperometric at 0.65 V to evaluate methanol poisoning were performed. For Pt/C electrode, the addition of methanol caused a rapid drop of the current due to CO poisoning. However, both FePc/H-BDDP-150 and Fe-C_3N_4/O-BDDP-650 samples showed excellent methanol tolerance (Fig. S7).

3.2.3. Computational calculations

The effect of the surface chemistry has been found to be critical, especially for the FePc catalyst supported on BDDP. The interaction with the different surfaces has produced a very distinct distribution of the FePc complexes. To deepen into these experimental observations, DFT calculations were performed to obtain some insights about the interaction of FePc and diamond surface.

Figs. 6a,b and Figs. 6e,F show the axial interactions between a FePc molecule with a cluster of diamond H-saturated and how the substitution of an atom of H for a -OH functional group affects the system. In the FePc macromolecule, iron is coordinated to the Pc by 4 nitrogen atoms. In the bottom, FePc interacts with the diamond cluster and the upper position remains free for the interaction with molecular O_2 in the ORR. It was observed that the distance between the two flakes was reduced almost 0.4 Å when the -OH functional group is present, which means that a stronger interaction is taking place after the substitution. However, the stabilization energy when O is present is low (~0.1 eV) as the H atoms of the (111) surface are still hindering the interaction. Also, when oxygen functional group is present, the FePc is reoriented for a better interaction of the phthalocyanine center with the oxygen (Figs. 6c,d). Despite the reorientation of FePc, the Fe-O coordination is not possible due to the strong repulsion caused by the H-terminated surface. The low interaction of the FePc molecule with the H-saturated surface agrees with the poor stability observed in the durability test for FePc/H-BDDP-150 sample. Fig. S8 shows the interaction of the FePc with a carbonyl substituted diamond cluster. In this case, the interaction observed was slightly lower. This might be related to the shorter bond distance in the carbonyl functional group ($C_{diamond}$=O: 1.25 Å) compared to the $C_{diamond}$-OH bond (1.47 Å), aggravating the H-surface hinderance to the FePc as the oxygen atom is closer to the diamond cluster.

The DFT results suggest that FePc in BDDP with oxygen functionalities may present higher durability as the interaction with this groups is stronger. However, the catalysts studied with oxidized surface chemistry (FePc/O-BDDP-150 and FePc/O-BDDP-650) showed much lower activity because FePc agglomeration occurs. This agglomeration might be taking place around the O-functional groups, where the FePc interacts stronger. Finally, the excellent electron transfer observed for FePc/H-BDDP-150 may be associated to the interaction of the FePc with the Csp^2 impurities as the interaction with the diamond surface is weak and the distance between flakes is not low enough for a proper electron transfer.

4. Conclusions

BDDP materials are emerging as very interesting carbon-based supports for electrocatalytic reactions where the durability of the material is limited by carbon corrosion due to the high potentials to which the electrode is exposed. Deep understanding of BDDP properties when used as catalyst support is important for the efficient design of robust catalysts for potential energy and environmental applications. In this case, we have focused on the role of BDDP properties on the catalytic performance of different Fe species towards the ORR.

The results show that the interaction between the active phase and the BDDP support determines the performance of the materials when modified with FePc or Fe-C_3N_4 species as it strongly influences the charge transfer between the support and the active sites. The electrocatalytic performance, especially for FePc species, was affected by the surface chemistry of the materials. In fact, the expected catalytic activity values for FePc systems were only observed for FePc/H-BDDP-150, while the FePc/O-BDDP samples presented much lower electron transfer. For Fe-C_3N_4 species, the main parameter affecting the catalytic performance was the particle size, where larger particles (O-BDDP-650) allowed a better and homogeneous formation of C_3N_4 layers and an excellent selectivity towards the 4-electron pathway. Probably, in this case, the temperature used for the synthesis of the Fe-C_3N_4 species minimizes the effect of the different surface chemistry.

Regarding the intrinsic electrocatalytic properties of iron coordinated by N, it was observed a superior performance of FePc than Fe-C_3N_4 in both selectivity and onset potentials. While the performance of FePc with just 1 wt.% of metal was almost equivalent to the commercial catalyst (20 wt.% of Pt), Fe-C_3N_4 showed poorer activity, which is coherent with other investigations that suggest that, with carbon nitride coordination, other metals may present higher activity towards the ORR, probably due to a more efficient ligand to metal center interaction.

CRediT author statement

Authors contributed equally to this work.

Declaration of Competing Interest

The authors declare that they have no known competing financial interests or personal relationships that could have appeared to influence the work reported in this paper.

Data availability

Data will be made available on request.

Acknowledgments

The authors would like to thank PID2019–105923RB-I00 and PID2021–123079OB-I00 projects funded by MCIN/AEI/10.13039/501100011033 and “ERDF A way of making Europe”. B. Martínez-Sánchez and G. Alemany-Molina thank Ministerio de Universidades for the FPU18/05127 and FPU20/03969 grants, respectively.

Supplementary materials

Supplementary material associated with this article can be found, in the online version, at doi:10.1016/j.electacta.2023.142121.

References

[1] M. Shao, Q. Chang, J.-P. Dodelet, R. Chenitz, Recent advances in electrocatalysts for oxygen reduction reaction, Chem. Rev. 116 (2016) 3594–3657, https://doi.org/10.1021/acs.chemrev.5b00462.
[2] T. Kondo, M. Kikuchi, H. Masuda, F. Katsumata, T. Aikawa, M. Yuasa, Boron-doped diamond powder as a durable support for platinum-based cathode catalysts in polymer electrolyte fuel cells, J. Electrochem Soc. 165 (2018) F3072–F3077, https://doi.org/10.1149/2.0111806jes.
[3] T. Kondo, Conductive boron-doped diamond powder/nanoparticles for electrochemical applications, Chem. Lett. 50 (2021) 733–741, https://doi.org/10.1246/CL.200870.
[4] J. Monzó, D.F. van der Vliet, A. Yanson, P. Rodriguez, Elucidating the degradation mechanism of the cathode catalyst of PEFCs by a combination of electrochemical methods and X-ray fluorescence spectroscopy, Phys. Chem. Chem. Phys. 18 (2016) 22407–22415, https://doi.org/10.1039/C6CP03795J.
[5] M. Winter, R.J. Brodd, What are batteries, fuel cells, and supercapacitors? Chem. Rev. 104 (2004) 4245–4270, https://doi.org/10.1021/cr020730k.
[6] J. Kim, Y.S. Chun, S.K. Lee, D.S. Lim, Improved electrode durability using a boron-doped diamond catalyst support for proton exchange membrane fuel cells, RSC Adv. 5 (2015) 1103–1108, https://doi.org/10.1039/C4RA13389G.
[7] T. Matsunaga, T. Kondo, T. Osasa, A. Kotsugai, I. Shitanda, Y. Hoshi, M. Itagaki, T. Aikawa, T. Tojo, M. Yuasa, Sensitive electrochemical detection of ciprofloxacin

at screen-printed diamond electrodes, Carbon 159 (2020) 247–254, https://doi.org/10.1016/j.carbon.2019.12.051.
[8] L. Ostrovskaya, V. Perevertailo, V. Ralchenko, A. Dementjev, O. Loginova, Wettability and surface energy of oxidized and hydrogen plasma-treated diamond films, Diam. Relat. Mater. 11 (2002) 845–850, https://doi.org/10.1016/S0925-9635(01)00636-7.
[9] D.A. Tryk, K. Tsunozaki, T.N. Rao, A. Fujishima, Relationships between surface character and electrochemical processes on diamond electrodes: dual roles of surface termination and near-surface hydrogen, Diam. Relat Mater. 10 (2001) 1804–1809, https://doi.org/10.1016/S0925-9635(01)00453-8.
[10] T. Kondo, H. Sakamoto, T. Kato, M. Horitani, I. Shitanda, M. Itagaki, M. Yuasa, Screen-printed diamond electrode: a disposable sensitive electrochemical electrode, Electrochem. Commun. 13 (2011) 1546–1549, https://doi.org/10.1016/j.elecom.2011.10.013.
[11] J.L. Figueiredo, M.F.R. Pereira, M.M.A. Freitas, J.J.M. Órfao, Modification of the surface chemistry of activated carbons, Carbon 37 (1999) 1379–1389, https://doi.org/10.1016/S0008-6223(98)00333-9.
[12] T. Ishii, S. Kashihara, Y. Hoshikawa, J. Ozaki, N. Kannari, K. Takai, T. Enoki, T. Kyotani, A quantitative analysis of carbon edge sites and an estimation of graphene sheet size in high-temperature treated, non-porous carbons, Carbon 80 (2014) 135–145, https://doi.org/10.1016/j.carbon.2014.08.048.
[13] McEnaney, B., Lahaye, J., Ehrburger, P., Active sites in relation to gasification of coal chars, in: (Eds.), Fundamental Issues in Control of Carbon Gasification Reactivity, Vol. 192, Ch. 4, Springer Netherlands, Dordrecht, 1991, pp. 175–203. 10.1007/978-94-011-3310-4_10.
[14] A. Gabe, R. Ruiz-Rosas, E. Morallón, D. Cazorla-Amorós, Understanding of oxygen reduction reaction by examining carbon-oxygen gasification reaction and carbon active sites on metal and heteroatoms free carbon materials of different porosities and structures, Carbon 148 (2019) 430–440, https://doi.org/10.1016/j.carbon.2019.03.092.
[15] A. Shen, Y. Zou, Q. Wang, R.A.W. Dryfe, X. Huang, S. Dou, L. Dai, S. Wang, Oxygen reduction reaction in a droplet on graphite: direct evidence that the edge is more active than the basal plane, Angew. Chem. Int. Ed. 53 (2014) 10804–10808, https://doi.org/10.1002/anie.201406695.
[16] G. Zhong, H. Wang, H. Yu, H. Wang, F. Peng, Chemically drilling carbon nanotubes for electrocatalytic oxygen reduction reaction, Electrochim. Acta 190 (2016) 49–56, https://doi.org/10.1016/j.electacta.2015.12.216.
[17] M. Seredych, A. Szczurek, V. Fierro, A. Celzard, T.J. Bandosz, Electrochemical Reduction of Oxygen on Hydrophobic Ultramicroporous PolyHIPE Carbon, ACS Catal 6 (2016) 5618–5628, https://doi.org/10.1021/acscatal.6b01497.
[18] J.H. Zagal, S. Griveau, K.I. Ozoemena, T. Nyokong, F. Bedioui, Carbon nanotubes, phthalocyanines and porphyrins: attractive hybrid materials for electrocatalysis and electroanalysis, J. Nanosci. Nanotechnol. 9 (2009) 2201–2214, https://doi.org/10.1166/jnn.2009.SE15.
[19] J.H. Zagal, F. Bedioui, Electrochemistry of N4 Macrocyclic Metal Complexes, 2nd Ed, 2, Springer International Publishing, Cham, 2016, https://doi.org/10.1007/978-3-319-31332-0.
[20] M.S. Dresselhaus, A. Jorio, A.G. Souza Filho, R. Saito, Defect characterization in graphene and carbon nanotubes using Raman spectroscopy, Philos. Trans. R. Soc. A Math. Phys. Eng. Sci. 368 (2010) 5355–5377, https://doi.org/10.1098/rsta.2010.0213.
[21] A. Santidrián, J.M. González-Domínguez, V. Diez-Cabanes, J. Hernández-Ferrer, W. K. Maser, A.M. Benito, A. Anśon-Casaos, J. Cornil, T. da Ros, M. Kalbáč, A tool box to ascertain the nature of doping and photoresponse in single-walled carbon nanotubes, Phys. Chem. Chem. Phys. 21 (2019) 4063–4071, https://doi.org/10.1039/C8CP06961A.
[22] A. Kaniyoor, S. Ramaprabhu, A Raman spectroscopic investigation of graphite oxide derived graphene, AIP Adv. 2 (2012), 032183, https://doi.org/10.1063/1.4756995.
[23] E. Mahé, D. Devilliers, C. Comninellis, Electrochemical reactivity at graphitic micro-domains on polycrystalline boron doped diamond thin-films electrodes, Electrochim. Acta 50 (2005) 2263–2277, https://doi.org/10.1016/j.electacta.2004.10.060.
[24] J.K. Nørskov, J. Rossmeisl, A. Logadottir, L. Lindqvist, J.R. Kitchin, T. Bligaard, H. Jónsson, Origin of the overpotential for oxygen reduction at a fuel-cell cathode, J. Phys. Chem. B. 108 (2004) 17886–17892, https://doi.org/10.1021/jp047349j.
[25] E. Raymundo-Piñero, D. Cazorla-Amorós, A. Linares-Solano, J. Find, U. Wild, R. Schlögl, Structural characterization of N-containing activated carbon fibers prepared from a low softening point petroleum pitch and a melamine resin, Carbon 40 (2002) 597–608, https://doi.org/10.1016/S0008-6223(01)00155-5.
[26] W. Ju, A. Bagger, G.-.P. Hao, A.S. Varela, I. Sinev, V. Bon, B. Roldan Cuenya, S. Kaskel, J. Rossmeisl, P. Strasser, Understanding activity and selectivity of metal-nitrogen-doped carbon catalysts for electrochemical reduction of CO_2, Nat. Commun. 8 (2017) 944, https://doi.org/10.1038/s41467-017-01035-z.
[27] L.P. Lv, Z.S. Wu, L. Chen, H. Lu, Y.R. Zheng, T. Weidner, X. Feng, K. Landfester, D. Crespy, Precursor-controlled and template-free synthesis of nitrogen-doped carbon nanoparticles for supercapacitors, RSC Adv. 5 (2015) 50063–50069, https://doi.org/10.1039/C5RA06697B.
[28] O. Ornelas, J.M. Sieben, R. Ruiz-Rosas, E. Morallón, D. Cazorla-Amorós, J. Geng, N. Soin, E. Siores, B.F.G. Johnson, On the origin of the high capacitance of nitrogen-containing carbon nanotubes in acidic and alkaline electrolytes, Chem. Commun. 50 (2014) 11343–11346, https://doi.org/10.1039/C4CC04876H.
[29] A. Alsudairi, J. Li, N. Ramaswamy, S. Mukerjee, K.M. Abraham, Q. Jia, Resolving the iron phthalocyanine redox transitions for ORR catalysis in aqueous media, J. Phys. Chem. Lett. 8 (2017) 2881–2886, https://doi.org/10.1021/acs.jpclett.7b01126.
[30] J.H. Zagal, Metallophthalocyanines as catalysts in electrochemical reactions, Coord. Chem. Rev. 119 (1992) 89–136, https://doi.org/10.1016/0010-8545(92)80031-L.
[31] J.H. Zagal, M.T.M. Koper, Reactivity descriptors for the activity of molecular MN4 catalysts for the oxygen reduction reaction, Angew. Chem. 128 (2016) 14726–14738, https://doi.org/10.1002/ange.201604311.
[32] X. Wan, X. Liu, Y. Li, R. Yu, L. Zheng, W. Yan, H. Wang, M. Xu, J. Shui, Fe–N–C electrocatalyst with dense active sites and efficient mass transport for high-performance proton exchange membrane fuel cells, Nat. Catal. 2 (2019) 259–268, https://doi.org/10.1038/s41929-019-0237-3.
[33] L. Jiao, G. Wan, R. Zhang, H. Zhou, S. Yu, H. Jiang, From metal–organic frameworks to single-atom fe implanted n-doped porous carbons: efficient oxygen reduction in both alkaline and acidic media, Angew. Chem. Int. Ed. 57 (2018) 8525–8529, https://doi.org/10.1002/anie.201803262.
[34] J.D. Yi, R. Xu, Q. Wu, T. Zhang, K.T. Zang, J. Luo, Y.L. Liang, Y.B. Huang, R. Cao, Atomically dispersed iron–nitrogen active sites within porphyrinic triazine-based frameworks for oxygen reduction reaction in both alkaline and acidic media, ACS Energy Lett. 3 (2018) 883–889, https://doi.org/10.1021/acsenergylett.8b00245.
[35] S. Fu, C. Zhu, D. Su, J. Song, S. Yao, S. Feng, M.H. Engelhard, D. Du, Y. Lin, Porous carbon-hosted atomically dispersed iron–nitrogen moiety as enhanced electrocatalysts for oxygen reduction reaction in a wide range of pH, Small 14 (2018), 1703118, https://doi.org/10.1002/smll.201703118.
[36] G. Alemany-Molina, J. Quílez-Bermejo, M. Navlani-García, E. Morallón, D. Cazorla-Amorós, Efficient and cost-effective ORR electrocatalysts based on low content transition metals highly dispersed on C3N4/super-activated carbon composites, Carbon 196 (2022) 378–390, https://doi.org/10.1016/j.carbon.2022.05.003.
[37] X. Chen, R. Hu, DFT-based study of single transition metal atom doped g-C_3N_4 as alternative oxygen reduction reaction catalysts, Int. J. Hydrog. Energy. 44 (2019) 15409–15416, https://doi.org/10.1016/j.ijhydene.2019.04.057.
[38] K. Chen, K. Liu, P. An, H. Li, Y. Lin, J. Hu, C. Jia, J. Fu, H. Li, H. Liu, Z. Lin, W. Li, J. Li, Y.R. Lu, T.S. Chan, N. Zhang, M. Liu, Iron phthalocyanine with coordination induced electronic localization to boost oxygen reduction reaction, Nat. Commun. 11 (2020) 4173, https://doi.org/10.1038/s41467-020-18062-y.
[39] B. Martínez-Sánchez, D. Cazorla-Amorós, E. Morallón, P-functionalized carbon nanotubes promote highly stable electrocatalysts based on Fe-phthalocyanines for oxygen reduction: experimental and computational studies, J. Energy Chem. 72 (2022) 276–290, https://doi.org/10.1016/J.JECHEM.2022.05.024.
[40] S. Kasahara, K. Natsui, T. Watanabe, Y. Yokota, Y. Kim, S. Iizuka, Y. Tateyama, Y. Einaga, Surface hydrogenation of boron-doped diamond electrodes by cathodic reduction, Anal. Chem. 89 (2017) 11341–11347, https://doi.org/10.1021/acs.analchem.7b02129.
[41] X. Yan, X. Xu, Z. Zhong, J. Liu, X. Tian, L. Kang, J. Yao, The effect of oxygen content of carbon nanotubes on the catalytic activity of carbon-based iron phthalocyanine for oxygen reduction reaction, Electrochim. Acta. 281 (2018) 562–570, https://doi.org/10.1016/j.electacta.2018.05.183.
[42] M.J. Bleda-Martínez, D. Lozano-Castelló, E. Morallón, D. Cazorla-Amorós, A. Linares-Solano, Chemical and electrochemical characterization of porous carbon materials, Carbon 44 (2006) 2642–2651, https://doi.org/10.1016/j.carbon.2006.04.017.
[43] X. Lu, W.L. Yim, B.H.R. Suryanto, C. Zhao, Electrocatalytic oxygen evolution at surface-oxidized multiwall carbon nanotubes, J. Am. Chem. Soc. 137 (2015) 2901–2907, https://doi.org/10.1021/ja509879r.
[44] M.J. Bleda-Martínez, J.A. Maciá-Agulló, D. Lozano-Castelló, E. Morallón, D. Cazorla-Amorós, A. Linares-Solano, Role of surface chemistry on electric double layer capacitance of carbon materials, Carbon 43 (2005) 2677–2684, https://doi.org/10.1016/j.carbon.2005.05.027.
[45] L.A. Hutton, J.G. Iacobini, E. Bitziou, R.B. Channon, M.E. Newton, J. v. Macpherson, Examination of the factors affecting the electrochemical performance of oxygen-terminated polycrystalline boron-doped diamond electrodes, Anal. Chem. 85 (2013) 7230–7240, https://doi.org/10.1021/ac401042t.
[46] J. Zagal, P. Bindra, E. Yeager, A mechanistic study of o_2 reduction on water soluble phthalocyanines adsorbed on graphite electrodes, J. Electrochem. Soc. 127 (1980) 1506–1517, https://doi.org/10.1149/1.2129940.
[47] C. González-Gaitán, R. Ruiz-Rosas, E. Morallón, D. Cazorla-Amorós, Relevance of the interaction between the m-phthalocyanines and carbon nanotubes in the electroactivity toward ORR, Langmuir 33 (2017) 11945–11955, https://doi.org/10.1021/acs.langmuir.7b02579.